Published in final edited form as:

J Neurochem. 2018 November ; 147(3): 395–408. doi:10.1111/jnc.14553.

Dysregulation of schizophrenia-related aquaporin 3 through disruption of paranode influences neuronal viability

Kazuo Kunisawa[1,7], **Takeshi Shimizu**[1,7,8], **Itaru Kushima**[2], **Branko Aleksic**[2], **Daisuke Mori**[2,3], **Yasuyuki Osanai**[1,7], **Kenta Kobayashi**[4,7], **Anna M. Taylor**[5], **Manzoor A. Bhat**[5], **Akiko Hayashi**[6], **Hiroko Baba**[6], **Norio Ozaki**[2], and **Kazuhiro Ikenaka**[1,7]

[1]Division of Neurobiology and Bioinformatics, National Institute for Physiological Sciences, Okazaki 444-8787, Japan

[2]Department of Psychiatry, Nagoya University Graduate School of Medicine, Nagoya 466-8550, Japan

[3]Brain and Mind Research Center, Nagoya University, Nagoya 466-8550, Japan

[4]Section of Viral Vector Development, National Institute for Physiological Sciences, Okazaki 444-8585, Japan

[5]Department of Cellular and Integrative Physiology, School of Medicine, University of Texas Health Science Center, San Antonio 78229-3900, USA

[6]Department of Molecular Neurobiology, Tokyo University of Pharmacy and Life Sciences, Hachioji 192-0392, Japan

[7]SOKENDAI (The Graduate University for Advanced Studies), Okazaki 444-8787, Japan

Abstract

Myelinated axons segregate the axonal membrane into four defined regions: the node of Ranvier, paranode, juxtaparanode and internode. The paranodal junction consists of specific component proteins, such as neurofascin155 (NF155) on the glial side, and Caspr and Contactin on the axonal side. Although paranodal junctions are thought to play crucial roles in rapid saltatory conduction and nodal assembly, the role of their interaction with neurons is not fully understood. In a previous study, conditional *NF155* knockout in oligodendrocytes led to disorganization of the paranodal junctions. To examine if disruption of paranodal junctions affects neuronal gene expression, we prepared total RNA from the retina of *NF155* conditional knockout, and performed expression

Address correspondence and reprint requests to Takeshi Shimizu, Department of Neurophysiology and Brain Science, Graduate School of Medical Sciences, Nagoya City University, Nagoya, Aichi 467-8601, Japan. tshimizu@med.nagoya-cu.ac.jp.

[8]Present address: Department of Neurophysiology and Brain Science, Graduate School of Medical Sciences, Nagoya City University, Nagoya, Aichi 467-8601, Japan

DR. KAZUO KUNISAWA (Orcid ID : 0000-0002-4786-9681)

DR. TAKESHI SHIMIZU (Orcid ID : 0000-0003-1041-1199)

Conflict of interest disclosure: The authors declare a conflict of interest that Kazuhiro Ikenaka is the current president of the ISN.

Supporting information

Additional Supporting Information may be found online in the supporting information tab for this article:

Figure S1. qRT-PCR analysis of the focused gene expression normalized by GAPDH in the retina or cerebral cortex of *Plp-NF155*$^{Flox/Flox}$ and *CST-KO* mice.

Figure S2. *AQP3* expression was also reduced in *PLP*$^{4e/-}$ mice, similarly to that in *Plp-NF155*$^{Flox/Flox}$ mice.

Figure S3. Confirmation of AQP3 overexpression in Neuro2A cells transfected with a plasmid-encoding *AQP3* gene.

analysis. We found that the expression level of 433 genes changed in response to paranodal junction ablation. Interestingly, expression of *aquaporin 3* (*AQP3*) was significantly reduced in *NF155* conditional knockout mice, but not in cerebroside sulfotransferase knockout (*CST-KO*) mice, whose paranodes are not originally formed during development. Copy number variations (CNVs) have an important role in the etiology of schizophrenia (SCZ). We observed rare duplications of *AQP3* in SCZ patients, suggesting a correlation between abnormal *AQP3* expression and SCZ. To determine if *AQP3* overexpression in *NF155* conditional knockout mice influences neuronal function, we performed adeno-associated virus (AAV)-mediated overexpression of *AQP3* in the motor cortex of mice and found a significant increase in caspase-3-dependent neuronal apoptosis in *AQP3*-transduced cells. This study may provide new insights into therapeutic approaches for SCZ by regulating *AQP3* expression, which is associated with paranodal disruption.

Graphical Abstract

The aquaporin 3 was related to the list of genes identified with copy number variations of schizophrenia, suggesting a correlation between abnormal aquaporin 3 expression and schizophrenia. We found that aquaporin 3 was sensitive to paranodal abnormalities. We further showed that dysregulation of aquaporin 3 expression through disruption of paranode affected neuronal viability. Further understanding of aquaporin 3 function may provide new insights into the etiology of schizophrenia caused by oligodendrocyte abnormalities and potential therapeutic approaches.

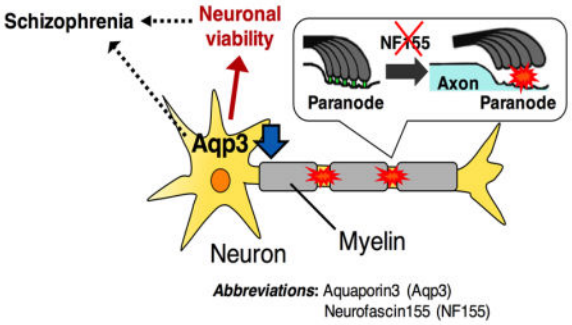

Keywords

paranodal junction; neurofascin155; aquaporin 3; schizophrenia; multiple sclerosis; copy number variant

Introduction

Oligodendrocytes are glial cells that myelinate neuronal axons in the central nervous system (CNS). Myelin insulates axons to increase conduction velocity of neuronal action potentials (Nave 2010). Myelin is also important for neuronal maintenance by metabolically supporting axons through transport of lactate or pyruvate (Lee *et al.* 2012).

An imbalance of the inhibitory-excitatory activities within the neural network in the CNS can cause psychiatric diseases (Cui *et al.* 2016). White matter abnormalities can also play

roles in psychiatric diseases, especially during the juvenile and adolescent periods (White *et al.* 2016). Several studies have demonstrated that a decrease in oligodendrocyte number and altered expression of myelin/oligodendrocyte-related genes in schizophrenia (SCZ) patients could affect white matter morphology and neuronal connectivity, which are characteristic features of SCZ (Martins-de-Souza *et al.* 2009). Recent studies have shown that several proteins localized to the nodes of Ranvier, such as neurofascin, contactins and ankyrin G, are also affected in SCZ (Roussos *et al.* 2012). In addition, some studies have shown that reduced expression of these junctional proteins leads to axonal degeneration even in the absence of gross demyelination (Taylor *et al.* 2017; Saifetiarova *et al.* 2017). Paranodal junctions are also known to execute several functions including the maintenance of action potential propagation (Rasband *et al.* 1999), segregation of axonal surface proteins (Rios *et al.* 2003), and signal transduction between axon and glia (Michailov *et al.* 2004). Combined, these data suggest that pathological changes in the white matter are causative factors of SCZ.

Overexpression of *proteolipid protein 1* (*PLP*), a major component of the myelin sheath, causes oligodendrocyte dysfunction in $PLP^{4e/-}$ mice (Kagawa *et al.* 1994), including abnormal paranodal junctions during the early phase (Tanaka *et al.* 2009) and later demyelination. Our previous studies have reported that early phase $PLP^{4e/-}$ mice display behavioral abnormalities related to cognitive dysfunction, which is one of the characteristic features of SCZ-like behaviors (Tanaka *et al.* 2009). It has also been reported that social isolation of both young and adult mice leads to behavioral and cognitive dysfunction, partially caused by myelination defects in the prefrontal cortex (Makinodan *et al.* 2012; Liu *et al.* 2012). Conversely, administration of a drug that enhances myelination to socially isolated mice rescues the behavioral changes and improves myelination in the prefrontal cortex (Liu *et al.* 2016). These findings suggest that myelination plays essential roles in cognitive function in these mouse models.

Recently, Yamazaki *et al.* (2010) showed that depolarization of an oligodendrocyte modulates the conduction velocity of the axons myelinated by the oligodendrocyte. Therefore, oligodendrocytes/myelin actively communicate with axons to modulate various properties of the neurons. Given that individual oligodendrocytes can myelinate multiple axons from the motor cortex and sensory cortex in the corpus callosum (Osanai *et al.* 2017), it is possible that oligodendrocytes mediate information processing between these cortical regions. This could explain the poor cognitive function caused by white matter abnormalities. Furthermore, conduction velocity deficits can influence the expression of oligodendroglial and neuronal genes (Roussos *et al.* 2012). Combined, these reports suggest that the disruption of oligodendroglial paranodal junctions influences their counterpart axons, eventually affecting neuronal gene expression and function. However, this hypothesis remains to be tested.

In this study, we investigated how neurons are affected by the disruption of paranodal junctions on their axons. We took advantage of conditional ablation of *NF155* in myelinating oligodendrocytes (*Plp-CreERT;NF155*$^{Flox/Flox}$ mice; Doerflinger *et al.* 2003; Pillai *et al.* 2009). The mice display a gradual loss of paranodal junctions and a concomitant disorganization of axonal domains (Pillai *et al.* 2009). We found that the expression level of various neuronal genes changed in response to the ablation of paranodal junctions.

Interestingly, we found that the expression of some genes in *Plp-CreERT;NF155$^{Flox/Flox}$* mice significantly differed from controls, but were unaffected in cerebroside sulfotransferase knockout (*CST-KO*) mice, whose paranodes fail to form during development. Copy number variations (CNVs), a major source of genetic variation in the human genome, are an important factor in the risk for SCZ (Stewart *et al.* 2011). Here, we identified that duplications of *aquaporin3* (*AQP3*), whose expression was decreased in *Plp-CreERT;NF155$^{Flox/Flox}$* mice, were significantly associated with risk of SCZ. We further demonstrated that *AQP3* overexpression in *Plp-CreERT;NF155$^{Flox/Flox}$* mice led to an increase in both neuronal swelling and caspase-3-dependent apoptosis. These findings suggest that the abnormal *AQP3* expression affects neuronal viability and may be involved in the pathogenesis of SCZ caused by oligodendrocyte abnormalities.

Material and methods

Animals

No blinding, no randomization and no sample calculation were performed. This study was not pre-registered. The transgenic mice of both sexes (body weight; 25–35 g) used in this study were generated and genotyped as described previously: *Plp-CreERT;NF155$^{Flox/Flox}$* mice (Doerflinger *et al.* 2003; Pillai *et al.* 2009); cerebroside sulfotransferase knockout mice (*CST-KO* mice; RRID: IMSR_RBRC00962; Ishibashi *et al.* 2002; Honke *et al.* 2002); *proteolipid protein 1* transgenic mice (*PLP$^{4e/-}$* mice; Kagawa *et al.* 1994). *Plp-CreERT;NF155$^{Flox/Flox}$* mice and the tissues obtained from *CST-KO* mice were kindly provided by Dr. Manzoor A. Bhat (University of Texas Health Science Center) and Dr. Hiroko Baba (Tokyo University of Pharmacy and Life Sciences), respectively. All mice were housed at mouse cage (345×168×140 mm) in a temperature-controlled room (24–25 °C) with a 12 : 12 light–dark cycle. Mice were fed ad libitum. All procedures were conducted in accordance with the guidelines defined by the National Institutes of Health Guide for the Care and Use of Laboratory Animals, and the National Institute for Physiological Sciences Animal Care and Use Committee (reference number; 17A086, 17A087).

Tamoxifen treatment

Tamoxifen administration experiments were carried out according to a previous report (Pillai *et al.* 2009). In brief, Tamoxifen (Cat# 205-14363, Wako, Osaka, Japan) was dissolved at 10 mg/ml in sunflower oil by sonicating at 36°C for 30 minutes. *Plp-CreERT;NF155$^{+/Flox}$* or *Plp-CreERT;NF155$^{Flox/Flox}$* mice were intraperitoneally injected with 10 mg/ml tamoxifen for 10 consecutive days beginning at P23. We refer to them hereafter as *Plp-NF155$^{+/Flox}$* and the *Plp-NF155$^{Flox/Flox}$* mice, respectively. The animals were then sacrificed at various time points as described in the Results section.

Mouse tissue preparation

For histological analysis, mice were deeply anesthetized with an intraperitoneal injection of sodium pentobarbital (70 mg/kg) and perfused transcardially with 4% paraformaldehyde (PFA) in 0.1 M sodium phosphate buffer. Brains were post-fixed in 4% paraformaldehyde overnight at 4°C. The optic nerves were post-fixed in 4% paraformaldehyde for 1 min at room temperature. The post-fixed tissues were cryoprotected in PBS containing 20% sucrose

overnight, embedded in OCT compound (Cat# 4583, Sakura Finetechnical Co., Tokyo, Japan), and cut into 20 μm (brain) or 10 μm (optic nerve) sections using a cryostat (CM3050S, Leica CM3050, Wetzlar, Germany) for *in situ* hybridization and immunohistochemistry.

In situ hybridization

Digoxigenin (DIG)-labeled single stranded riboprobes for *AQP3* (GenBank Accession Number, NM_016689) were synthesized using T7 RNA polymerase and DIG RNA labeling mix (Cat# 11277073910, Roche, Mannheim, Germany). The protocol for *in situ* hybridization was previously described (Ma *et al.* 2006). Briefly, the sections were treated with proteinase K (40 μg/ml for 30 min at room temperature; Cat# 107393, Merck, USA) and hybridized overnight at 60°C with DIG-labeled antisense riboprobes in a hybridization solution consisting of 40% formamide, 20 mM Tris-HCl (pH 7.5), 600 mM NaCl, 1 mM EDTA, 10% dextran sulfate, 200 μg/ml yeast tRNA, 1× Denhardt's solution, and 0.25% SDS. The sections were washed three times in 1× SSC (150 mM NaCl and 15 mM sodium citrate) containing 50% formamide at 60°C, followed by 0.1 M maleic buffer (pH 7.5) containing 0.1% Tween 20 and 0.15 M NaCl. The bound DIG-labeled probe was detected by overnight incubation with anti-DIG antibody conjugated with alkaline phosphatase (Cat# 11093274910, Roche), and the color was developed in a solution containing 4-nitro-blue tetrazolium chloride (NBT, Cat# 11383213001, Roche) and 5-bromo-4-chloro-3-indolyl phosphate (BCIP, Cat# 11383221001, Roche) in the dark at room temperature.

Immunohistochemistry

Cryosections were immunostained with mouse anti-NeuN antibody (1:1,000; Cat# MAB377, Millipore, Billerica, USA), rabbit anti-GFP antibody (1:500; Cat# A6455, Life Technologies, Carlsbad, USA), rabbit anti-NF155 antibody (1:500; a gift from Dr. Hiroko Baba, Tokyo University of Pharmacy and Life Sciences, Japan), rabbit anti-Caspr antibody (1:1,000; a gift from Dr. Elior Peles, Weizmann Institute of Science, Israel), and rabbit anti-AQP3 antibody (1:200; Cat# sc-20811, Santa Cruz Biotechnology, Dallas, USA). Sections were irradiated in 10 mM citrate buffer (pH 6.0) for 5 min, heated up to 90°C in a microwave. After washing with PBS containing 0.1% Triton-X (PBST), sections were blocked with 10% normal goat serum in PBST for 1 h, then incubated with primary antibodies in PBST at 4°C overnight. After washing with PBST, the sections were incubated with secondary antibodies (1:2000; Alexa488-conjugated goat anti-mouse IgG (Cat# A-11001), Alexa488-conjugated goat anti-rabbit IgG (Cat# A-11008), Alexa568-conjugated goat anti-mouse IgG (Cat# A-11004), and Alexa568-conjugated goat anti-rabbit IgG (Cat# A-11011); Molecular Probes, Eugene, USA) and Hoechst 33342 (0.1 μg/ml; Cat# H6024, Sigma-Aldrich, St. Louis, USA) for 3 h at room temperature. Sections were mounted and covered with glass coverslips after rinsing with PBST.

Sections used for 3,3′-diaminobenzidine (DAB) staining were blocked with 10% normal goat serum in PBST for 30 min, then incubated with rabbit anti-Cleaved Caspase-3 antibody (1:400; Cat# 9661, Cell Signaling Technology, Danvers, USA) at 4°C overnight. After washing with PBST, the sections were incubated with secondary antibody (1:400, biotinylated goat anti-rabbit IgG; Cat# BA-1000, Vector Laboratories, CA, USA) for 1 h at

room temperature, followed by incubation with Avidin/Biotin Complex (ABC) solution (horseradish peroxidase-streptavidin-biotin complex, Vectastain ABC kit; Cat# PK-6100, Vector Laboratories) for 1 h at room temperature. The HRP signals were detected by DAB solution with 0.03% H_2O_2. Cell areas were defined as surrounding the outer border of an EGFP-positive cell body using ImageJ software.

RT-PCR and qRT-PCR

Total RNA was isolated using a Sepasol G kit (Cat# 09379, Nacalai Tesque, Kyoto, Japan) according to the manufacturer's instructions. The first-strand cDNA was synthesized using ReverTra Ace (Cat# TRT-101, Toyobo, Osaka, Japan). PCR was performed using KAPA Taq Extra PCR kit (Cat# KK3606, Kapa Biosystems, Wilmington, USA). For the quantitative PCR, SYBR Master Mix Reagent (Cat# 04707516001, Takara, Otsu, Japan) was used and then subjected to real time PCR quantification using an ABI7300 (Applied Biosystems, Waltham, USA). Quantitative PCR analysis was performed using a StepOne analyzer (Life Technologies). The PCR reaction program consisted of 40 cycles of denaturation at 95°C for 15 s and annealing and elongation at 60°C for 1 min. To discriminate specific amplification from non-specific amplification, melting curve analysis was performed after each PCR reaction. To determine the starting amount of cDNA, each purified PCR product of known concentration was serially diluted and used as a standard. β-actin was used as a housekeeping gene to normalize all PCR data; GAPDH was also used as an additional internal control for further confirmation in *Plp-NF155*$^{Flox/Flox}$ mice and *CST-KO* mice (Figure S1). All PCR primer sequences are described in Table 1.

Expression analysis in response to the disruption of paranodal junctions

Total RNA prepared from mouse retina was isolated using NucleoSpin RNA kit (Cat# 740955, Takara) according to the manufacturer's instructions. Total RNA concentration was measured spectrophotometrically with a NanoDrop. The quality of purified total RNA was verified by an Agilent 2100 bioanalyzer (Agilent technologies, Santa Clara, USA). Isolated total RNA was amplified and labeled according to a previously described method in the One-Color Microarray-Based Gene Expression Microarrays Analysis Protocol (Agilent Technologies). Briefly, total RNA (100 ng) was converted into cDNA using the Low Input Quick Amp Labeling Kit (Cat# 5190, Agilent Technologies), followed by *in vitro* transcription and incorporation of Cyanine 3-CTP into cRNA. Cyanine 3-labeled cRNA was purified using RNeasy Mini kit (Cat# 74104, Qiagen, Hilden, Germany). After fragmentation, labelled cRNA was hybridized to SurePrint G3 Mouse Gene Expression 8×60K Microarray (Cat# G4858A, Agilent Technologies) for 17 h at 65°C. The microarray was scanned by an Agilent Scanner, and the scan image data was analyzed with Feature Extraction software (Agilent Technologies). After background signal subtraction, the data for two microarray samples was managed and analyzed using the GeneSpring GX software (Agilent Technologies). A total of 55,821 probes were used for this analysis. Raw intensity values were normalized to the 50-percentile shift and then subjected to a Bayesian correction based on the median of the control samples. Altered transcripts were identified using the comparative method with the $\log_2$ normalized intensity values between *Plp-NF155*$^{Flox/Flox}$ mouse and control samples.

Genetic analysis of candidate genes in schizophrenia patients

Expression analysis revealed that over 400 genes were differentially up-regulated or down-regulated between *Plp-NF155*$^{Flox/Flox}$ and *Plp-NF155*$^{+/Flox}$ mice. For genetic analysis in SCZ patients, we manually extracted genes which exert an effect on neuronal function. Furthermore, we focused on two gene candidates whose expression was altered only in *Plp-NF155*$^{Flox/Flox}$ mice, but not in *CST-KO* mice, and explored whether the candidate genes were associated with a risk for SCZ. We examined the published CNV datasets of SCZ cases and psychiatrically normal controls (Kushima *et al.* 2017). In brief, we analyzed 1699 cases with SCZ and 824 psychiatrically normal controls using high-resolution (> 10 kb) array comparative genomic hybridization (aCGH). Genomic DNA extracted from blood or saliva samples was used in CNV analysis. NimbleGen 720k Whole-Genome Tiling arrays were used for genome-wide CNV screening. CNV calls were made with Nexus Copy Number software v.7.5 (BioDiscovery, El Segundo, USA) using the Fast Adaptive States Segmentation Technique 2 algorithm, which is a hidden Markov model-based approach. Differences in frequency of CNVs between cases and controls were evaluated using the one-sided Fisher's exact test, with significance set at $p < 0.05$.

Transfection of expression vectors into Neuro2A

Mouse AQP3 (NM_016689) cDNA was cloned from female mouse brain total RNA by RT-PCR. pCX-EGFP vector was purchased from Clontech Laboratories (Cat# 15007, CA, USA). AQP3-2A-peptide-EGFP and EGFP cDNAs were constructed using the AQP3 and/or pCX-EGFP constructs as backbone. To construct pAAV-AQP3-2A-EGFP and pAAV-EGFP, the AQP3-2A-peptide-EGFP or EGFP cDNAs were subcloned into the pAAV vector. Neuro2A cells were grown in Dulbecco's modified Eagle's medium (DMEM; Cat# 08456, Nacalai Tesque, Kyoto, Japan) supplemented with 10% fetal bovine serum (FBS; Cat# 2917254, MP Biomedicals, Santa Ana, USA), and 1% penicillin/streptomycin (PS; Cat# 15140122, Gibco, Grand Island, USA), and maintained at 37°C in a humidified atmosphere with 5% CO_2. One day before transfection, Neuro2A (2.0×10^5 cells per well) were seeded onto glass coverslips in 6-well tissue culture plates and transfected with pAAV-EGFP or pAAV-AQP3-2A-EGFP vectors using Lipofectamine 2000 reagent (Cat# 11668027, Invitrogen, Carlsbad, USA). We diluted 2.0 μg of DNA in 250 μL Opti-MEM™ medium (Cat# 31985070, Invitrogen) and 5 μL of Lipofectamine 2000 reagent in 250 μL Opti-MEM™ without serum, and combined the diluted DNA and diluted Lipofectamine 2000 (total volume was 500 μL). The transfection complex (500 μL) was applied to each well containing Neuro2A cells in 2 mL of growth medium without antibiotics. After 4 h of incubation, the medium was changed to growth medium and the cells were maintained for an additional 48 h.

Immunocytochemistry

Cells were fixed with 4% paraformaldehyde in 0.1 M PBS for 10 min and then permeabilized with 0.1% Triton X-100 for an additional 10 min. After incubation in blocking solution (1% goat serum/PBS) for 1 h, mouse rabbit anti-AQP3 (1:200; Cat# sc-20811, Santa Cruz Biotechnology) and rat anti-GFP (1:1,000; Cat# 04404-84, Nacalai Tesque, Kyoto, Japan) antibodies diluted in blocking solution were applied and incubated

overnight at 4°C. After washing in PBS, cells were incubated with secondary antibodies (1:2000; Alexa568-conjugated goat anti-rabbit IgG (Cat# A-11011) and Alexa488-conjugated goat anti-rat IgG (Cat# A-11006); Molecular Probes) and Hoechst 33342 (0.1 μg/ml; Sigma) for 3 h at room temperature. Immunofluorescent signals were observed under a Nikon A1R Confocal Microscope (Tokyo, Japan).

Adeno-associated virus (AAV) production and purification

All adeno-associated virus (AAV) vectors were produced and purified as described previously (Matsushita *et al.* 1998; Okada *et al.* 2005; Kobayashi *et al.* 2016). In brief, HEK293 cells (3×10^6 cells in a 10 cm tissue culture dish) were co-transfected with pAAV vector plasmid harboring a gene of interest, pAAV-RC2, and pHelper (Cat# VPK-422 and VPK-402, Cell Biolabs, Inc, San Diego, USA). The crude viral lysate was purified with 2 rounds of cesium chloride ultracentrifugation. The titer of the viral stock was determined against plasmid standards by real-time PCR with primers 5′-CCGTTGTCAGGCAACGTG-3′ and 5′-AGCTGACAGGTGGTGGCAAT-3′; subsequently, the stock was dissolved in HN buffer (50 mM HEPES [pH 7.4] and 0.15 M NaCl) and stored at −80°C.

AAV injection into the mouse motor cortex

We injected AAV2-EGFP or AAV2-AQP3-2A-EGFP into the motor cortex of *Plp-CreERT;NF155*$^{+/Flox}$ and *Plp-CreERT;NF155*$^{Flox/Flox}$ mice 50 days after tamoxifen treatment. Mice were anesthetized with an intraperitoneal injection of ketamine/xylazine solution (100 mg/kg and 5 mg/kg, respectively) and placed in a stereotaxic frame (Cat# SR-5M-HT, Narishige, Tokyo, Japan) with a mouse adapter. After opening the skull at the injection site, 0.2 – 0.25 μl of viral solution (0.5×10^9 viral genome [vg]) was injected into the motor cortex (0.5 mm anterior and 1.2 mm lateral to the bregma, at a depth of 0.4 mm) through pulled glass pipettes (outer diameter 40 – 60 μm) using an air pressure system, which took about 3 min. The pipette was withdrawn 3 min after the viral administration. Incisions were closed using wound clips. The mice were sacrificed 30 days after AAV injection.

Data analyses

All statistics were analyzed with GraphPad Prism 6 Software (GraphPad Software, Inc., San Diego, USA). Significant differences in comparisons of the two groups were evaluated using Student's t-test. Multiple group comparisons were performed by one-way ANOVA followed by Tukey's post hoc tests. The criterion for a significant difference was $p < 0.05$ for all statistical evaluation. Data presented showed all the replicates and as the mean ± SEM. To evaluate the difference in frequencies of clinically significant CNVs between SCZ cases and controls, *p*-values were calculated with a one-sided Fisher's exact test.

Results

Expression profiles of neuronal genes in response to disruption of paranodal junctions

Disruption of paranodal junctions occurs during the early phase of demyelinating diseases (Çolakoğlu *et al.* 2014). It is possible that disruption of paranodal junctions can affect

neuronal gene expression. To address this hypothesis, we took advantage of a tamoxifen inducible-Cre line, *Plp-CreERT*, in which Cre expression is specifically induced in proteolipid protein (PLP)-positive mature oligodendrocytes. When *Plp-CreERT* mice are mated with *NF155*$^{Flox/Flox}$ mice, the combined *Plp-CreERT;NF155*$^{Flox/Flox}$ mice allow for tamoxifen-induced ablation of the *NF155* gene in mature oligodendrocytes during postnatal development (Doerflinger *et al.* 2003; Pillai *et al.* 2009). *Plp-CreERT;NF155*$^{Flox/Flox}$ and age-matched *Plp-CreERT;NF155*$^{+/Flox}$ mice were intraperitoneally injected with tamoxifen for 10 consecutive days, from P23 to P33 (Fig. 1a). These are hereafter referred to as *Plp-NF155*$^{Flox/Flox}$ and *Plp-NF155*$^{+/Flox}$ mice, respectively (see Methods and Materials). Previous studies have shown that NF155 immunoreactivity was significantly diminished by 60 days after tamoxifen administration in the peripheral nervous system (Pillai *et al.* 2009; Fig. 1a). To investigate neuronal gene expression in response to paranodal junction disruption, we performed Agilent GeneChip analysis on recombinant retinal tissues 60 days after tamoxifen treatment. The mouse retina contains the neuronal cell bodies of the optic nerves. In addition, myelin is absent in the retina because astrocytes form a honeycomb-like structure called the lamina cribrosa adjacent to the retinal region. Therefore, retinal tissue which does not contact oligodendrocytes is useful for extracting neuronal gene expression affected by the disruption of paranodal junctions. To confirm the loss of paranodal junctions in the optic nerves of *Plp-NF155*$^{Flox/Flox}$ mice, immunostaining for NF155 and Caspr was performed in the optic nerves (Fig. 1b). In *Plp-NF155*$^{Flox/Flox}$ mice 60 days after tamoxifen administration, both the number and length of NF155^{+} clusters were significantly reduced compared to *Plp-NF155*$^{+/Flox}$ mice (number, $p < 0.001$; length, $p < 0.05$; Fig. 1c and d). We also observed an apparent decrease in Caspr-positive signals in the optic nerves of *Plp-NF155*$^{Flox/Flox}$ mice (number and length, $p < 0.01$; Fig. 1e and f). These results are consistent with previous studies showing that *NF155* mutations induce disruption of the paranodal junctions in the peripheral nervous system (Pillai *et al.* 2009).

To examine gene expression profiles in the retina of *Plp-NF155*$^{Flox/Flox}$ mice, expression analysis was performed with total retinal RNA isolated from *Plp-NF155*$^{+/Flox}$ or *Plp-NF155*$^{Flox/Flox}$ mice 60 days after tamoxifen administration. The expression level of various neuronal genes was significantly changed in response to the ablation of the paranodal junctions (Fig. 1g). The expression levels of 433 genes showed more than a two-fold difference between *Plp-NF155*$^{Flox/Flox}$ and *Plp-NF155*$^{+/Flox}$ mice. Among these 433 genes, 228 genes were up-regulated and the remainder were down-regulated. To validate the results obtained by expression analysis, total RNA was extracted from the retina of *Plp-NF155*$^{Flox/Flox}$ mice and used for quantitative RT-PCR (qRT-PCR). Among the identified genes, we focused on six gene candidates with the following criteria: (i) more than 6 in the normalized intensity values of *Plp-NF155*$^{+/Flox}$ and *Plp-NF155*$^{Flox/Flox}$ mice; (ii) more than two-fold difference between *Plp-NF155*$^{+/Flox}$ and *Plp-NF155*$^{Flox/Flox}$ mice; (iii) genes expected for exerting an effect on neuronal function. These focal genes are indicated in Fig. 1g: *decorin* (*DCN*), *myosin heavy polypeptide 11* (*MYH11*), *pituitary tumor-transforming gene 1* (*PTTG1*), *dopachrome tautomerase* (*DCT*), *TELO2 interacting protein 2* (*TTI2*), and *aquaporin 3* (*AQP3*). *DCN* and *MYH11* are neuronal survival factors signaling through TGF-β and IGF-1 (Iozzo *et al.* 2011; Renard *et al.* 2013), respectively. *PTTG1* and *DCT* are involved in tumor development (Lee *et al.* 1999; Pak *et al.* 2004), whereas *TTI2* is a

regulator of the DNA damage response (Hurov *et al.* 2010), and *AQP3* functions in the transport of water molecules within a cell (Preston *et al.* 1992). The primers used for PCR amplification are listed in Table 1. The up- or down-regulation of gene expression detected by qRT-PCR was identical to that obtained in the expression analysis, supporting our expression profiles (*DCN*, *MYH11*, *DCT*, *TTI2*, and *AQP3*, $p < 0.05$; *PTTG1*, $p < 0.01$; Fig. 1h and i). These findings suggest that neuronal function is affected by the altered gene expression caused by paranodal abnormalities.

Comparison of retinal gene expression between *Plp-NF155$^{Flox/Flox}$* and *CST-KO* mice in response to paranodal disruption

The expression analysis indicated that the gradual loss of paranodal junctions after their initial formation alters neuronal gene expression. We next examined whether expression levels of our focal genes were also affected in another mutant mouse line whose paranodes never form during development. This mutant mouse line lacks the cerebroside sulfotransferase (CST) enzyme, which synthesizes sulfatide, one of the major lipid components of the myelin sheath (Eckhardt *et al.* 2007). Ishibashi *et al.* (2002) reported that *CST* mutant mice do not form paranodal junctions during development but show normal ion channel localizations on axons until 6 weeks of age. Previous studies have shown that *CST-KO* mice undergo a switch from axonal voltage-dependent sodium channel (Nav) 1.2 to Nav1.6 during development (Suzuki *et al.* 2004), while increased amounts of Nav1.2 and its aberrant localization are observed in *PLP$^{4e/-}$* mice, whose paranodes are disrupted after initial formation (Rasband *et al.* 2003). Since dysregulation of axonal Nav isoforms can influence neuronal function, we compared the expression levels of our focal genes in the retina of 4- or 6-week-old *CST-KO* mice to those of *Plp-NF155$^{Flox/Flox}$* mice 40 or 60 days after tamoxifen administration. While *DCN* and *MYH11* expression were also induced in *CST-KO* mice (compared to *Plp-NF155$^{Flox/Flox}$* mice: *DCN* and *MYH11*, $p < 0.05$; *CST-KO* mice: *DCN* (6w) and *MYH11* (6w), $p < 0.05$, *DCN* (4w), $p < 0.01$; Fig. 2a–d), the response of the other focal genes differed between *Plp-NF155$^{Flox/Flox}$* and *CST-KO* mice. The expression of *PTTG1* and *AQP3* was significantly altered in *Plp-NF155$^{Flox/Flox}$* mice (*PTTG1*, $p < 0.01$; *AQP3*, $p < 0.05$; Fig. 2e and g) but not in *CST-KO* mice (*PTTG1* and *AQP3*, $p > 0.05$; Fig. 2f and h). These data indicate that some genes are only affected by disruption of paranodes after their initial formation, but not by an initial lack of paranodal development.

AQP3, whose expression is decreased by paranodal disruption, is linked to schizophrenia by CNV analysis

We previously reported that SCZ-related behaviors in mice are associated with abnormal paranodal structures (Tanaka *et al.* 2009). In SCZ patients, the disruption of myelin, including the paranodal junction, occurs after its initial formation (Roussos *et al.* 2012). Therefore, we investigated whether *PTTG1* and *AQP3* genes identified in our expression analysis were linked to CNV of SCZ. Intriguingly, the locus encoding *AQP3* displayed a characteristic CNV pattern. We found that duplications of the *AQP3* locus were detected in eight SCZ patients (n = 1699), but not in controls (n = 824; Fig. 3a). The excess of the duplications in SCZ cases was statistically significant (one-sided Fisher's exact test $p = 0.042$). We identified no CNVs at the *PTTG1* locus. Together SCZ-related behaviors in mice

are associated with abnormal paranodal structures (Tanaka *et al.* 2009), our CNV analyses suggest that the reduction in *AQP3* expression caused by paranodal disruption may function in the pathogenesis of SCZ.

AQP3 overexpression in the motor cortex of *Plp-NF155$^{Flox/Flox}$* mice decreases cell volume and induces caspase-3 activation

AQP3 was one of the genes highly down-regulated in the retina of *Plp-NF155$^{Flox/Flox}$* mice, but not in *CST-KO* mice. AQP3 has been reported to control the cellular uptake of H_2O and influence intracellular signaling in mammalian cells (Galán-Cobo *et al.* 2015). Moreover, AQP-mediated water transport is involved in brain volume regulation, cerebrospinal fluid movement and metabolism (Verkman 2005). We therefore examined whether AQP3 expression is also affected in the cerebral cortex of *Plp-NF155$^{Flox/Flox}$* mice in addition to the retina. qRT-PCR analysis revealed a significant decrease in *AQP3* expression in the cortex of *Plp-NF155$^{Flox/Flox}$* mice ($p < 0.05$; Fig. 3b). In our previous study using demyelinating *PLP$^{4e/-}$* mice, slightly abnormal paranodal structures were observed at 2 months of age (Tanaka *et al.* 2009). We found that *AQP3,* whose expression was altered in *Plp-NF155$^{Flox/Flox}$* mice but not in *CST-KO* mice, was also downregulated in the cortex of 2-month-old *PLP$^{4e/-}$* mice ($p < 0.05$; Figure S2). In contrast, *AQP3* mRNA levels were unchanged in the cerebral cortex of *CST-KO* mice compared to controls ($p > 0.05$; Fig. 3c). The reduced expression of *AQP3* in *Plp-NF155$^{Flox/Flox}$* mice was further confirmed by *in situ* hybridization (Fig. 3d). These results demonstrate that *AQP3* expression is also affected by disruption of paranodal junctions in the cerebral cortex. Next, to examine if AQP3 is expressed in neurons, we performed double immunostaining with anti-AQP3 and anti-NeuN (neuron marker) antibodies (Fig. 3e). In the *Plp-NF155$^{+/Flox}$* mice, the majority of NeuN-positive neurons had detectable AQP3 immunoreactivity (Fig. 3e and f), while *Plp-NF155$^{Flox/Flox}$* mice displayed reduced AQP3 expression in NeuN-positive neurons ($p < 0.001$; Fig. 3e and f). We found that about 90% of NeuN-positive cells in the cerebral cortex of *Plp-NF155$^{+/Flox}$* mice were positive for AQP3, indicating that AQP3 is primarily expressed in neurons (Fig. 3f). Furthermore, we found that the ratio of $AQP3^+/NeuN^+$ double-positive cells was significant decrease in the cerebral cortex of *Plp-NF155$^{Flox/Flox}$* mice ($p < 0.001$; Fig. 3f), and the decrease was more pronounced in the deeper layers of the cerebral cortex ($p < 0.001$; Fig. 3f). Thus, it is possible that the disruption of paranodal junctions affects neuronal function through the decrease in AQP3 expression.

Previous studies have shown that dysregulation of AQP directly controls cell death based on changes in cellular volume (Holm *et al.* 2016). The combination of these reports and the CNV data from the present study suggests a link between alterations in AQP3 expression and neuronal dysfunction. To further address this possibility, we utilized adeno-associated virus (AAV) injection *in vivo* to determine if overexpression of AQP3 in *Plp-NF155$^{Flox/Flox}$* mice, in which AQP3 expression is reduced, can be implicated in cellular viability. First, to confirm the expression of AQP3 by AAV, Neuro2A cells were transfected with a plasmid encoding the *AQP3* gene (pAAV-AQP3-2A-EGFP), and the expression level of AQP3 was compared with control plasmid-transduced cells (pAAV-EGFP). qRT-PCR analysis showed that *AQP3* mRNA significantly increased following transfection with pAAV-AQP3-2A-EGFP ($p < 0.05$; Figure S3a). Representative immunofluorescent images of AQP3 in AQP3

AAV vector-transduced or control Neuro2A cells indicated that AQP3 protein levels were also increased (Figure S3b). Therefore, we injected AAV2-AQP3-2A-EGFP or its control AAV2-EGFP bilaterally into the motor cortex of *Plp-NF155*$^{+/Flox}$ and *Plp-NF155*$^{Flox/Flox}$ mice 50 days after tamoxifen treatment and visualized AQP3-transduced neurons by GFP expression (Fig. 4a). Thirty days after AAV2-AQP3-2A-EGFP injection, we observed overexpression of *AQP3* in the motor cortex by *in situ* hybridization (Fig. 4b). Furthermore, EGFP-positive signals were abundant in the cortical neurons of the motor cortex (Fig. 4c). To address the effect of AQP3 overexpression on cell volume in *Plp-NF155*$^{Flox/Flox}$ mice, cell area was defined based on EGFP fluorescence intensity (Fig. 4d). In *Plp-NF155*$^{+/Flox}$ mice, AQP3 overexpression did not alter cell area ($p > 0.05$; Fig. 4e), in contrast to *Plp-NF155*$^{Flox/Flox}$ mice in which overexpression of AQP3 significantly decreased cell area ($p < 0.001$; Fig. 4e). This suggests that AQP3 overexpression under conditions of paranodal disruption may influence neuronal viability via cellular swelling or water homeostasis. We thus examined whether AQP3 overexpression in *Plp-NF155*$^{Flox/Flox}$ mice impacts caspase-3-dependent apoptosis. AQP3 overexpression in *Plp-NF155*$^{+/Flox}$ mice had only a slight effect on cleaved caspase-3-positive cells ($p > 0.05$; Fig. 4f and g), but induced a marked increase in the number of cleaved caspase-3-positive cells in *Plp-NF155*$^{Flox/Flox}$ mice compared to controls ($p < 0.001$; Fig. 4f and g). These results indicate that AQP3 overexpression under conditions of paranodal disruption increases neuronal swelling and caspase-3-dependent apoptosis. Together with the CNV data in the present study, these results suggest that abnormal AQP3 expression influences neuronal viability and contributes to SCZ.

Discussion

Demyelinating diseases are typical examples of diseases associated with white matter abnormalities. In general, demyelinating diseases are classified as neurological diseases but not psychiatric diseases. However, cognitive dysfunction is observed in patients experiencing demyelination (Malkki 2015), and white matter abnormalities are found in many SCZ patients (White *et al.* 2016). In our previous study using demyelinating *PLP*$^{4e/-}$ mice, we observed cognitive dysfunction prior to the onset of demyelination (Tanaka *et al.* 2009). In this early stage of the disease, paranodal disruption was observed; thus, we speculated that mild white matter abnormalities, such as paranodal disruption, could result in symptoms observed in SCZ patients.

In this study, we performed expression analysis and qRT-PCR on mouse retinal tissue to explore how the neuronal cell body responds to paranodal disruption. The results revealed that over 400 genes were differentially up- or down-regulated more than two-fold from the control level (Fig. 1g). Interestingly, we observed differences in the expression profiles of several genes between *Plp-NF155*$^{Flox/Flox}$ and *CST-KO* mice (Fig. 2). For example, the expression levels of *AQP3* and *PTTG1* were altered in *Plp-NF155*$^{Flox/Flox}$ (Fig. 2e and g), but remained unchanged in *CST-KO* mice (Fig. 2f and h). These results suggest that some genes are sensitive to paranodal disruption after they are formed, but are not affected by the lack of initial paranodal development. Paranodal junctions act as a seal between the myelin sheath and the axon to isolate them from the extracellular environment (Bhat *et al.* 2001). Previous studies have suggested that structural paranodal abnormalities might allow reactive oxygen species (ROS) and proteases to invade the internodal space (Gonsette 2008;

Rosenbluth *et al.* 2013); and the disruption of paranodal junctions in mice results in axonal swelling (Pillai *et al.* 2009). In addition, organelle accumulation was found in the paranodal region flanked by the swollen lesions, a sign of disrupted axonal transport, which eventually leads to axonal degeneration (Garcia-Fresco *et al.* 2006). Although the precise molecular mechanisms underlying these events remain to be elucidated, these reports suggest that the disruption of paranodal junctions causes axonal transport deficits and induces cytotoxic stress. Some studies have suggested that sequential phase shifts in sodium channel clustering may affect neuronal properties (Girault and Peles, 2002). Nav1.2 first appears on the axons during development, and is replaced by Nav1.6 in mature neurons (Boiko *et al.* 2001). This transition from Nav1.2 to Nav1.6 occurs in *CST-KO* mice (Suzuki *et al.* 2004). Previous paper reports that the transition from Nav1.2 to Nav1.6 appears to be disturbed as early as 2 months of age in $PLP^{4e/-}$ mice (Rasband et al., 2003). In addition, our previous study reported that demyelinating $PLP^{4e/-}$ mice showed slightly abnormal paranodal structures at 2 months of age (Tanaka *et al.* 2009), and the density of Na^+ channel clusters was significantly affected in $PLP^{4e/-}$ mice than wildtype mice at the same age (Tanaka et al., 2006). So, we analyzed *AQP3* expression at 2 months of age in $PLP^{4e/-}$ mice. We found that *AQP3,* whose expression was altered in $Plp\text{-}NF155^{Flox/Flox}$ mice but not in *CST-KO* mice, was also downregulated in the cortex of 2-month-old $PLP^{4e/-}$ mice ($p < 0.05$; Figure S2). Although it is unclear why the gene expression responses are different between $Plp\text{-}NF155^{Flox/Flox}$ and *CST-KO* mice, it is possible that the gradual loss of paranodal junctions after its formation might cause neuronal stress and change neuronal characters or functions. Further studies will be required to reveal the gene regulation in response to either early or late disruption of paranode. Microarray analysis comparing $Plp\text{-}NF155^{Flox/Flox}$ and *CST-KO* mouse data might be helpful to identify molecular mechanisms underlying these different gene expressions.

Immunostaining showed that AQP3 was primarily expressed in neurons (Fig. 3e and f). Moreover, expression of *AQP3* in the cerebral cortex was significantly decreased in $Plp\text{-}NF155^{Flox/Flox}$ mice compared to $Plp\text{-}NF155^{+/Flox}$ mice (Fig. 3b and c), and the decrease was more pronounced in the deeper layers of the cerebral cortex (Fig. 3f). Cortical neurons in different layers show different profiles of myelination (Tomassy *et al.* 2014). The lowest levels of myelin correspond to upper layers, whereas deeper layer neurons are the most densely myelinated (Tomassy *et al.* 2014). These findings suggest that the cortical neurons in the deeper layers are more markedly influenced by paranodal abnormalities. However, the functional role of AQP3 after the disruption of paranodal junctions has yet to be fully clarified. The up-regulation of AQP3 was observed in rat brains after focal cerebral ischemia and could contribute to the development of cerebral edema (Yang *et al.* 2009). Conversely, the down-regulation of AQP is essential for defending against severe oxidative stress, indicating potential clinical applications for AQP expression regulation (Te Velde *et al.* 2008). Here we suggest that the disruption of paranodal junctions influences neuronal function through a decrease in AQP3 expression. The reduction in AQP3 expression may be implicated in neuroprotection from cytotoxic stress caused by the disruption of paranodal junctions. Further studies on the function of AQP3 in $Plp\text{-}NF155^{Flox/Flox}$ mice will provide important insights into the roles of gene regulation during the disruption of paranodal junctions.

A growing number of recent reports have demonstrated the involvement of CNV in SCZ (Crespi *et al.* 2012). As one of the major sources of genetic variation, CNV provides a versatile tool for identifying candidate genes that may contribute to SCZ (Luo *et al.* 2014). In this study, by comparing the focal genes in our expression analysis to the list of genes identified with CNVs, we found changes in the expression of susceptibility genes associated with SCZ in response to paranodal disruption. Interestingly, these patients displayed rare duplications of the *AQP3* gene (Fig. 3a). We surmise that the duplication leads to increased gene expression. However, as we could not analyze gene expression levels in our CNV carriers, we are unable to examine whether the duplications actually affect *AQP3* gene expression. However, we demonstrated that *AQP3* overexpression after paranodal disruption induced the swelling of neurons and caspase-3-dependent apoptosis in motor cortex (Fig. 4d–g). Subsequent neuronal, dendritic and synaptic losses associated with increased caspase-3 levels were also found in patients with SCZ (Chen *et al.* 2009; Gassó *et al.* 2014). Structural and functional brain alterations are thought to underlie SCZ, and some of these alterations are observed in motor system (Walther *et al.* 2015). Previous studies have identified reduced volumes of the primary and secondary motor cortex in SCZ patients (Douaud *et al.* 2007; Wang *et al.* 2018). Furthermore, altered neuronal activity in the area was related to negative symptom of SCZ (Walther *et al.* 2017), suggesting that motor cortex may play a role in SCZ pathogenesis. Although it is difficult to examine whether or how the *AQP3* gene confers a risk for SCZ, abnormal *AQP3* expression may contribute to dysregulated motor network in SCZ.

In conclusion, our present study revealed that the gradual loss of paranodal junctions in *Plp-NF155*$^{Flox/Flox}$ mice altered neuronal gene expression (Fig. 1g). Based on the correlation between the focal genes identified in our expression analysis and CNV data for SCZ, *AQP3* is a candidate for a causative gene that shows rare duplications in SCZ patients (Fig. 3a). Given that abnormal *AQP3* expression in *Plp-NF155*$^{Flox/Flox}$ mice was implicated in neuronal viability (Fig. 4d–g), further understanding of AQP3 function may provide new insights into the etiology of SCZ and potential therapeutic approaches.

Supplementary Material

Refer to Web version on PubMed Central for supplementary material.

Acknowledgments

This work was supported by Grants-in-Aid for Scientific Research on Innovative Areas “Glial Assembly” (25117001) from the Ministry of Education, Culture, Sports, Science and Technology of Japan (MEXT); by the Strategic Research Program for Brain Sciences (SRPBS) from the Japan Agency for Medical Research and development, AMED; and by the Brain Mapping by Integrated Neurotechnologies for Disease Studies (Brain/MINDS) from the Japan Agency for Medical Research and Development, AMED. M.A.B. is supported by grants from the NIH NIGMS GM063074, National Multiple Sclerosis Society, and the Zachry Foundation (M.A.B). A.M.T. is supported by a NIH NINDS Postdoctoral Fellowship (F32NS092448). Confocal images were acquired at the Spectrography and Bioimaging Facility, National Institute for Basic Biology Core Research Facilities. We thank Dr. H. Sano, Dr. N. Hatanaka, and Prof. A. Nambu (National Institute for Physiological Sciences, Japan) for technical advice on injections into the motor cortex. We also thank our lab members for helpful discussions.

All experiments were conducted in compliance with the ARRIVE guidelines.

Abbreviations used

AAV	adeno-associated virus
AQP3	aquaporin3
CNS	central nervous system
CNV	copy number variant
CST	cerebroside sulfotransferase
DCN	decorin
DCT	dopachrome tautomerase
MYH11	myosin heavy polypeptide 11
MS	multiple sclerosis
Nav	voltage-dependent sodium channel
NF155	neurofascin155
NFASC	neurofascin
PLP	proteolipid protein
PTTG1	pituitary tumor-transforming gene 1
SCZ	schizophrenia
TTI2	TELO2 interacting protein 2

References

Bhat MA, Rios JC, Lu Y, Garcia-Fresco GP, Ching W, St Martin M, et al. Axon-glia interactions and the domain organization of myelinated axons requires neurexin IV/Caspr/Paranodin. Neuron. 2001; 30:369–383. [PubMed: 11395000]

Boiko T, Rasband MN, Levinson SR, Caldwell JH, Mandel G, Trimmer JS, Matthews G. Compact myelin dictates the differential targeting of two sodium channel isoforms in the same axon. Neuron. 2001; 30:91–104. [PubMed: 11343647]

Chen X, Sun C, Chen Q, O'Neill FA, Walsh D, Fanous AH, et al. Apoptotic engulfment pathway and schizophrenia. PLoS One. 2009; 4:e6875. [PubMed: 19721717]

Çolakoğlu G, Bergstrom-Tyrberg U, Berglund EO, Ranscht B. Contactin-1 regulates myelination and nodal/paranodal domain organization in the central nervous system. Proc Natl Acad Sci USA. 2014; 111:E394–403. [PubMed: 24385581]

Crespi BJ, Crofts HJ. Association testing of copy number variants in schizophrenia and autism spectrum disorders. J Neurodev Disord. 2012; 4:15. [PubMed: 22958593]

Cui LB, Liu K, Li C, Wang LX, Guo F, Tian P, et al. Putamen-related regional and network functional deficits in first-episode schizophrenia with auditory verbal hallucinations. Schizophr Res. 2016; 173:13–22. [PubMed: 26995674]

Doerflinger NH, Macklin WB, Popko B. Inducible site-specific recombination in myelinating cells. Genesis. 2003; 35:63–72. [PubMed: 12481300]

Douaud G, Smith S, Jenkinson M, Behrens T, Johansen-Berg H, Vickers J, et al. Anatomically related grey and white matter abnormalities in adolescent-onset schizophrenia. Brain. 2007; 130:2375–2386. [PubMed: 17698497]

Eckhardt M, Hedayati KK, Pitsch J, Lüllmann-Rauch R, Beck H, Fewou SN, Gieselmann V. Sulfatide storage in neurons causes hyperexcitability and axonal degeneration in a mouse model of metachromatic leukodystrophy. J Neurosci. 2007; 27:9009–9021. [PubMed: 17715338]

Garcia-Fresco GP, Sousa AD, Pillai AM, Moy SS, Crawley JN, Tessarollo L, et al. Disruption of axo-glial junctions causes cytoskeletal disorganization and degeneration of purkinje neuron axons. Proc Natl Acad Sci USA. 2006; 103:5137–5142. [PubMed: 16551741]

Galán-Cobo A, Ramírez-Lorca R, Serna A, Echevarría M. Overexpression of AQP3 modifies the cell cycle and the proliferation rate of mammalian cells in culture. PLoS One. 2015; 10:e0137692. [PubMed: 26367709]

Gassó P, Mas S, Molina O, Lafuente A, Bernardo M, Parellada E. Increased susceptibility to apoptosis in cultured fibroblasts from antipsychotic-naïve first-episode schizophrenia patients. J Psychiatr Res. 2014; 48:94–101. [PubMed: 24128664]

Girault JA, Peles E. Development of nodes of Ranvier. Curr Opn Neurobiol. 2002; 12:476–485.

Gonsette RE. Oxidative stress and excitotoxicity: a therapeutic issue in multiple sclerosis? Mult Scler. 2008; 14:22–34. [PubMed: 17881394]

Honke K, Hirahara Y, Dupree J, Suzuki K, Popko B, Fukushima J, et al. Paranodal junction formation and spermatogenesis require sulfoglycolipids. Proc Natl Acad Sci USA. 2002; 99:4227–4232. [PubMed: 11917099]

Holm A, Magnusson KE, Vikström E. Pseudomonas aeruginosa N-3-oxo-dodecanoyl-homoserine lactone elicits changes in cell volume, morphology, and AQP9 characteristics in macrophages. Front Cell Infect Microbiol. 2016; 6:32. [PubMed: 27047801]

Hurov KE, Cotta-Ramusino C, Elledge SJ. A genetic screen identifies the triple T complex required for DNA damage signaling and ATM and ATR stability. Genes Dev. 2010; 24:1939–1950. [PubMed: 20810650]

Iozzo RV, Buraschi S, Genua M, Xu SQ, Solomides CC, Peiper SC, et al. Decorin antagonizes IGF receptor I (IGF-IR) function by interfering with IGF-IR activity and attenuating downstream signaling. J Biol Chem. 2011; 286:34712–34721. [PubMed: 21840990]

Ishibashi T, Dupree JL, Ikenaka K, Hirahara Y, Honke K, Peles E, et al. A myelin galactolipid, sulfatide, is essential for maintenance of ion channels on myelinated axon but not essential for initial cluster formation. J Neurosci. 2002; 22:6507–6514. [PubMed: 12151530]

Kagawa T, Ikenaka K, Inoue Y, Kuriyama S, Tsujii T, Nakao J, et al. Glial cell degeneration and hypomyelination caused by overexpression of myelin proteolipid protein gene. Neuron. 1994; 13:427–442. [PubMed: 7520255]

Kobayashi K, Sano H, Kato S, Kuroda K, Nakamuta S, Isa T, et al. Survival of corticostriatal neurons by Rho/Rho-kinase signaling pathway. Neurosci Lett. 2016; 630:45–52. [PubMed: 27424794]

Kushima I, Aleksic B, Nakatochi M, Shimamura T, Shiino T, Yoshimi A, et al. High-resolution copy number variation analysis of schizophrenia in Japan. Mol Psychiatry. 2017; 22:430–440. [PubMed: 27240532]

Lee IA, Seong C, Choe IS. Cloning and expression of human cDNA encoding human homologue of pituitary tumor transforming gene. Biochem Mol Biol Int. 1999; 47:891–897. [PubMed: 10365261]

Lee Y, Morrison BM, Li Y, Lengacher S, Farah MH, Hoffman PN, et al. Oligodendroglia metabolically support axons and contribute to neurodegeneration. Nature. 2012; 487:443–448. [PubMed: 22801498]

Liu J, Dietz K, DeLoyht JM, Pedre X, Kelkar D, Kaur J, et al. Impaired adult myelination in the prefrontal cortex of socially isolated mice. Nat Neurosci. 2012; 15:1621–1623. [PubMed: 23143512]

Liu J, Dupree JL, Gacias M, Frawley R, Sikder T, Naik P, Casaccia P. Clemastine Enhances Myelination in the Prefrontal Cortex and Rescues Behavioral Changes in Socially Isolated Mice. J Neurosci. 2016; 36:957–962. [PubMed: 26791223]

Luo X, Huang L, Han L, Luo Z, Hu F, Tieu R, et al. Systematic prioritization and integrative analysis of copy number variations in schizophrenia reveal key schizophrenia susceptibility genes. Schizophr Bull. 2014; 40:1285–1299. [PubMed: 24664977]

Ma J, Matsumoto M, Tanaka KF, Takebayashi H, Ikenaka K. An animal model for late onset chronic demyelination disease caused by failed terminal differentiation of oligodendrocytes. Neuron Glia Biology. 2006; 2:81–91. [PubMed: 18634583]

Makinodan M, Rosen KM, Ito S, Corfas G. A critical period for social experience-dependent oligodendrocyte maturation and myelination. Science. 2012; 337:1357–1360. [PubMed: 22984073]

Malkki H. Multiple sclerosis: neuroimaging provides insights into cognitive dysfunction in MS. Nat Rev Neurol. 2015; 11:126. [PubMed: 25666745]

Martins-de-Souza D, Gattaz WF, Schmitt A, Rewerts C, Marangoni S, Novello JC, et al. Alterations in oligodendrocyte proteins, calcium homeostasis and new potential markers in schizophrenia anterior temporal lobe are revealed by shotgun proteome analysis. J Neural Transm. 2009; 116:275–289. [PubMed: 19034380]

Matsushita T, Elliger S, Elliger C, Podsakoff G, Villarreal L, Kurtzman GJ, et al. Adeno-associated virus vectors can be efficiently produced without helper virus. Gene therapy. 1998; 5:938–945. [PubMed: 9813665]

Michailov GV, Sereda MW, Brinkmann BG, Fischer TM, Haug B, Birchmeier C, et al. Axonal neuregulin-1 regulates myelin sheath thickness. Science. 2004; 304:700–703. [PubMed: 15044753]

Nave KA. Myelination and support of axonal integrity by glia. Nature. 2010; 468:244–252. [PubMed: 21068833]

Okada T, Nomoto T, Yoshioka T, Nonaka-Sarukawa M, Ito T, Ogura T, et al. Large-scale production of recombinant viruses by use of a large culture vessel with active gassing. Human Gene Therapy. 2005; 16:1212–1218. [PubMed: 16218782]

Osanai Y, Shimizu T, Mori T, Yoshimura Y, Hatanaka N, Nambu A, et al. Rabies virus-mediated oligodendrocyte labeling reveals a single oligodendrocyte myelinates axons from distinct brain regions. GLIA. 2017; 5:93–105.

Pak BJ, Lee J, Thai BL, Fuchs SY, Shaked Y, Ronai Z, Ben-David Y. Radiation resistance of human melanoma analysed by retroviral insertional mutagenesis reveals a possible role for dopachrome tautomerase. Oncogene. 2004; 23:30–38. [PubMed: 14712208]

Pillai AM, Thaxton C, Pribisko AL, Cheng JG, Dupree JL, Bhat MA. Spatiotemporal ablation of myelinating glia-specific neurofascin (Nfasc NF155) in mice reveals gradual loss of paranodal axoglial junctions and concomitant disorganization of axonal domains. J Neurosci Res. 2009; 87:1773–1793. [PubMed: 19185024]

Preston GM, Carroll TP, Guggino WB, Agre P. Appearance of water channels in Xenopus oocytes expressing red cell CHIP28 protein. Science. 1992; 256:385–387. [PubMed: 1373524]

Rasband MN, Peles E, Trimmer JS, Levinson SR, Lux SE, Shrager P. Dependence of nodal sodium channel clustering on paranodal axoglial contact in the developing CNS. J Neurosci. 1999; 19:7516–7528. [PubMed: 10460258]

Rasband MN, Kagawa T, Park EW, Ikenaka K, Trimmer JS. Dysregulation of axonal sodium channel isoforms after adult-onset chronic demyelination. J Neurosci Res. 2003; 73:465–70. [PubMed: 12898531]

Renard M, Callewaert B, Malfait F, Campens L, Sharif S, del Campo M, et al. Thoracic aortic-aneurysm and dissection in association with significant mitral valve disease caused by mutations in TGFB2. Int J Cardiol. 2013; 165:584–587. [PubMed: 23102774]

Rios JC, Rubin M, St Martin M, Downey RT, Einheber S, Rosenbluth J, et al. Paranodal interactions regulate expression of sodium channel subtypes and provide a diffusion barrier for the node of Ranvier. J Neurosci. 2003; 23:7001–7011. [PubMed: 12904461]

Rosenbluth J, Mierzwa A, Shroff S. Molecular architecture of myelinated nerve fibers: leaky paranodal junctions and paranodal dysmyelination. Neuroscientist. 2013; 19:629–641. [PubMed: 24122820]

Roussos P, Katsel P, Davis KL, Bitsios P, Giakoumaki SG, Jogia J, et al. Molecular and genetic evidence for abnormalities in the nodes of Ranvier in schizophrenia. Arch Gen Psychiatry. 2012; 69:7–15. [PubMed: 21893642]

Saifetiarova J, Taylor AM, Bhat MA. Early and late loss of the cytoskeletal scaffolding protein, Ankyrin G, reveals its role in maturation and maintenance of nodes of Ranvier in myelinated axons. J Neurosci. 2017; 37:2524–2538. [PubMed: 28148727]

Stewart LR, Hall AL, Kang SH, Shaw CA, Beaudet AL. High frequency of known copy number abnormalities and maternal duplication 15q11-q13 in patients with combined schizophrenia and epilepsy. BMC Med Genet. 2011; 12:154. [PubMed: 22118685]

Suzuki A, Hoshi T, Ishibashi T, Hayashi A, Yamaguchi Y, Baba H. Paranodal axoglial junction is required for the maintenance of the Nav1.6-type sodium channel in the node of Ranvier in the optic nerves but not in peripheral nerve fibers in the sulfatide-deficient mice. GLIA. 2004; 46:274–83. [PubMed: 15048850]

Tanaka H, Ikenaka K, Isa T. Electrophysiological abnormalities precede apparent histological demyelination in the central nervous system of mice overexpressing proteolipid protein. J Neurosci Res. 2006; 84:1206–16. [PubMed: 16917838]

Tanaka H, Ma J, Tanaka KF, Takao K, Komada M, Tanda K, et al. Mice with altered myelin proteolipid protein gene expression display cognitive deficits accompanied by abnormal neuron-glia interactions and decreased conduction velocities. J Neurosci. 2009; 29:8363–8371. [PubMed: 19571127]

Taylor AM, Saifetiarova J, Bhat MA. Postnatal loss of neuronal and glial neurofascins differentially affects node of Ranvier maintenance and myelinated axon function. Front Cell Neurosci. 2017; 11:11. [PubMed: 28217083]

Te Velde AA, Pronk I, de Kort F, Stokkers PC. Glutathione peroxidase 2 and aquaporin 8 as new markers for colonic inflammation in experimental colitis and inflammatory bowel diseases: an important role for H_2O_2? Eur J Gastroenterol Hepatol. 2008; 20:555–560. [PubMed: 18467915]

Tomassy GS, Berger DR, Chen HH, Kasthuri N, Hayworth KJ, Vercelli A, et al. Distinct profiles of myelin distribution along single axons of pyramidal neurons in the neocortex. Science. 2014; 344:319–24. [PubMed: 24744380]

Verkman AS. More than just water channels: unexpected cellular roles of aquaporins. J Cell Sci. 2005; 118:3225–3232. [PubMed: 16079275]

Walther S. Psychomotor symptoms of schizophrenia map on the cerebral motor circuit. Psychiatry Res. 2015; 233:293–298. [PubMed: 26319293]

Walther S, Stegmayer K, Federspiel A, Bohlhalter S, Wiest R, Viher PV. Aberrant Hyperconnectivity in the Motor System at Rest Is Linked to Motor Abnormalities in Schizophrenia Spectrum Disorders. Schizophr Bull. 2017; 43:982–992. [PubMed: 28911049]

Wang YM, Zou LQ, Xie WL, Yang ZY, Zhu XZ, Cheung EFC, Sørensen TA, Møller A, Chan RCK. Altered grey matter volume and cortical thickness in patients with schizo-obsessive comorbidity. Psychiatry Res Neuroimaging. 2018; 276:65–72. [PubMed: 29628272]

White T, Langen C, Schmidt M, Hough M, James A. Comparative neuropsychiatry: white matter abnormalities in children and adolescents with schizophrenia, bipolar affective disorder, and obsessive-compulsive disorder. Eur Psychiatry. 2015; 30:205–213. [PubMed: 25498242]

Yamazaki Y, Hozumi Y, Kaneko K, Fujii S, Goto K, Kato H. Oligodendrocytes: facilitating axonal conduction by more than myelination. Neuroscientist. 2010; 16:11–18. [PubMed: 19429890]

Yang M, Gao F, Liu H, Yu WH, Sun SQ. Temporal changes in expression of aquaporin-3, −4, −5 and −8 in rat brains after permanent focal cerebral ischemia. Brain Res. 2009; 1290:121–132. [PubMed: 19616516]

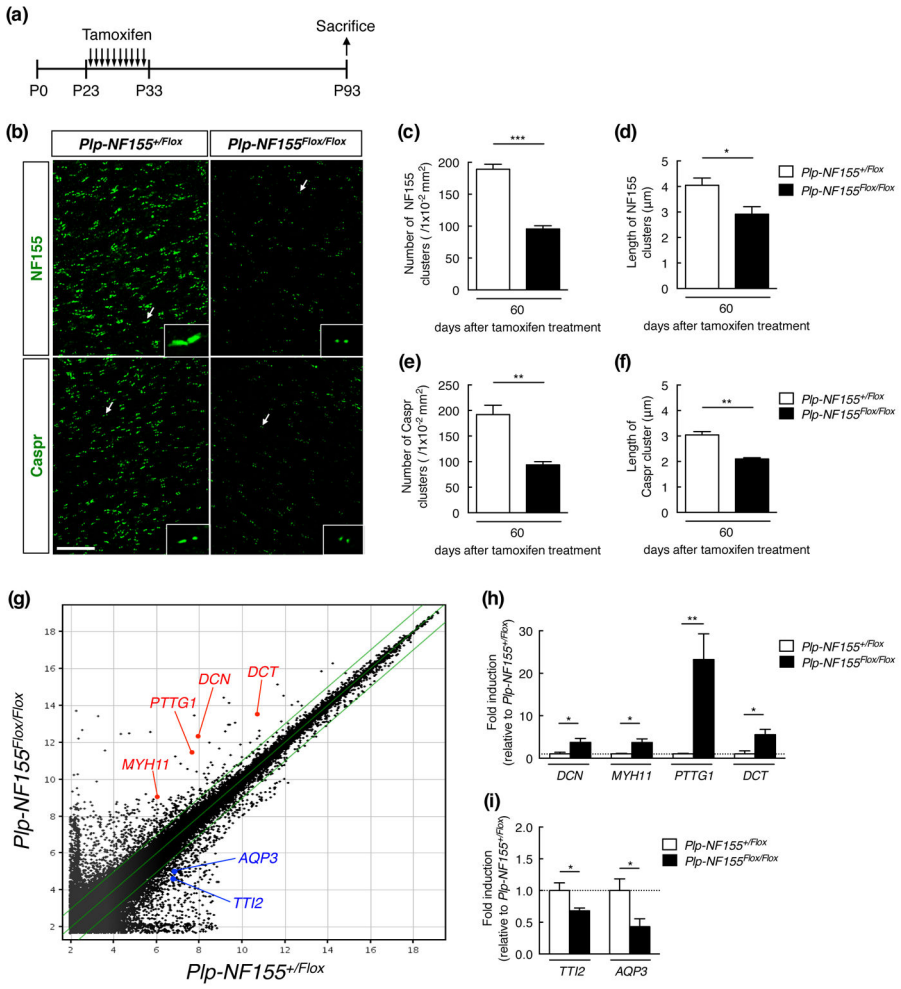

Fig. 1.

Expression analysis of total RNA prepared from the retina of *Plp-NF155*$^{+/Flox}$ or the *Plp-NF155*$^{Flox/Flox}$ mice. (a) Schematic of the experimental time course. (b) Examination of paranodal disruption in the optic nerves of *Plp-NF155*$^{Flox/Flox}$ mice 60 days after tamoxifen administration. Optic nerve sections were immunostained with anti-NF155 (upper panel) and anti-Caspr (lower panel) antibodies. The inset shows a magnified view of the immunolabeling indicated by the arrows. Scale bar: 40 μm. (c–f) Quantification of paranodal number and length. The sections were immunostained with anti-NF155 (c, d) or anti-Caspr (e, f) antibodies in *Plp-NF155*$^{+/Flox}$ and *Plp-NF155*$^{Flox/Flox}$ mice (*$p < 0.05$, **$p < 0.01$, **$p < 0.001$ compared to *Plp-NF155*$^{+/Flox}$ mice; Student's t-test; n = 3 mice each). (g) Neuronal gene expression in response to paranodal disruption. Total RNA was isolated from the retina of *Plp-NF155*$^{+/Flox}$ and *Plp-NF155*$^{Flox/Flox}$ mice (n = 2 per genotype) 60 days after tamoxifen administration and used for expression analysis. A scatter plot of gene expression levels in response to paranode ablation is shown. The normalized intensity values are represented by $\log_2$. The focal genes of this study are indicated by red (up-regulation) and blue (down-regulation) dots. The green line represents the boundary of a 2-fold change. (h, i) The expression levels of the identified genes in the *Plp-NF155*$^{+/Flox}$ and *Plp-NF155*$^{Flox/Flox}$ mice 60 days after tamoxifen administration were confirmed by qRT-PCR

(*$p < 0.05$, **$p < 0.01$ compared to *Plp-NF155*$^{+/Flox}$ mice; Student's t-test; n = 4–5 mice each).

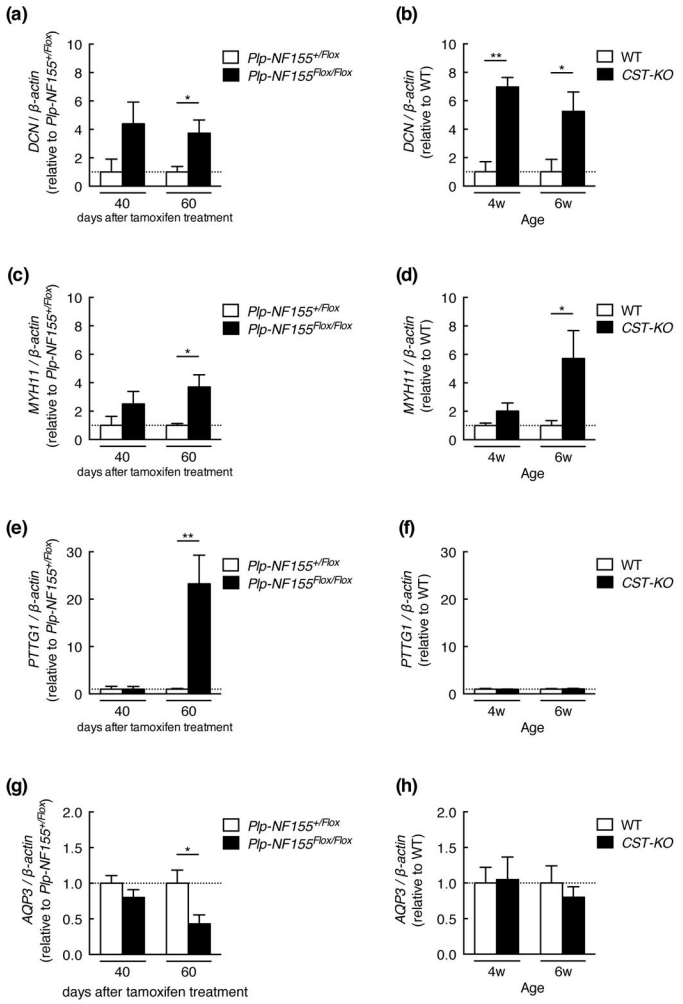

Fig. 2.

qRT-PCR analysis of the focused gene expression in the retina of *Plp-NF155*$^{Flox/Flox}$ and *CST-KO* mice. The expression levels of the focused genes normalized by β-actin in the retina of 4- or 6-week-old *CST-KO* mice (n = 4–5 mice each) or *Plp-NF155*$^{Flox/Flox}$ mice (n = 4–5 mice each) 40 or 60 days after tamoxifen administration were compared to *Plp-NF155*$^{+/Flox}$ mice. (a, b) The expression levels of *DCN* in *Plp-NF155*$^{Flox/Flox}$ mice (a) and *CST-KO* mice (b) were analyzed by qRT-PCR. (c, d) The expression levels of *MYH11* in *Plp-NF155*$^{Flox/Flox}$ mice (c) and *CST-KO* mice (d) were analyzed by qRT-PCR. (e, f) The expression levels of *PTTG1* in *Plp-NF155*$^{Flox/Flox}$ mice (e) and *CST-KO* mice (f) were analyzed by qRT-PCR. (g, h) The expression levels of *AQP3* in *Plp-NF155*$^{Flox/Flox}$ mice (g) and *CST-KO* mice (h) were analyzed by qRT-PCR. *$p < 0.05$, **$p < 0.01$ compared to *Plp-NF155*$^{+/Flox}$ mice or wild-type mice (Student's t-test).

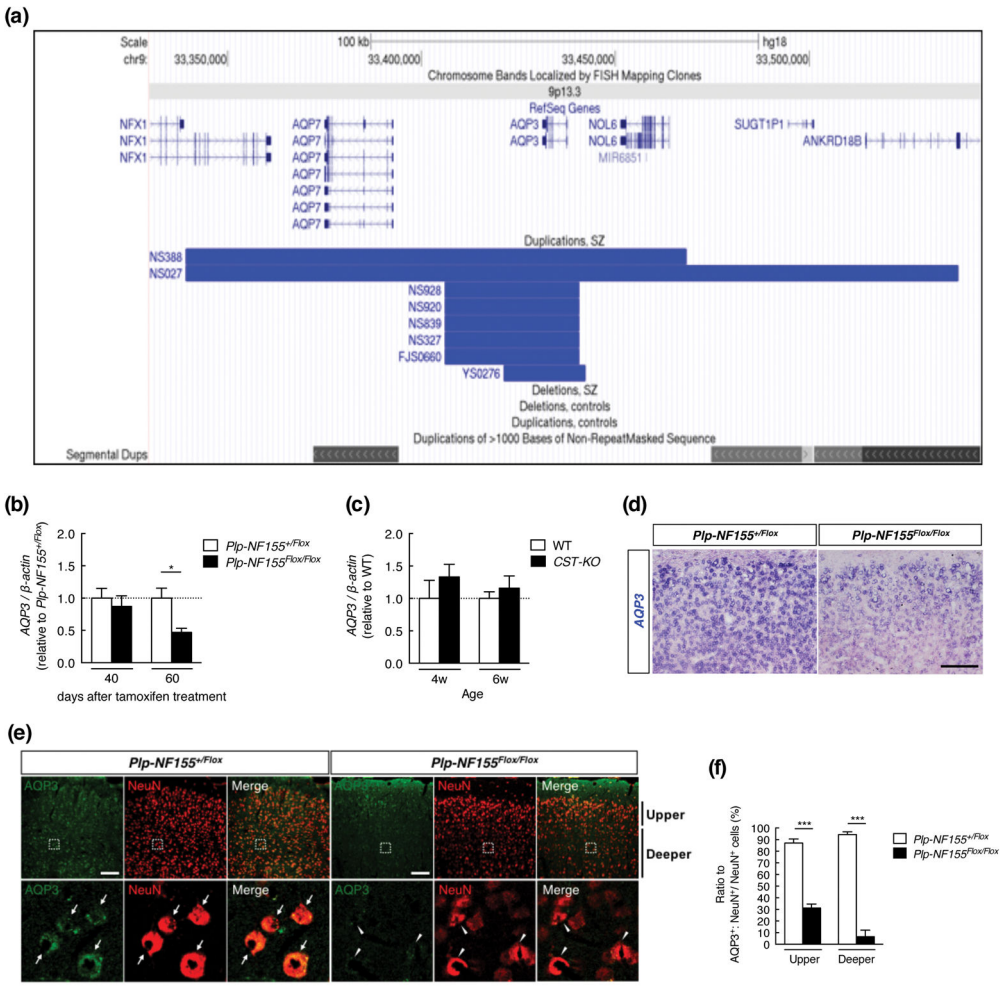

Fig. 3.

Duplications in the *AQP3* locus were found in patients with schizophrenia, corresponding to the decreased expression of AQP3 in *Plp-NF155*$^{Flox/Flox}$ mice. (a) Schematic drawing of the CNV positions in the *AQP3* locus. Duplications of the *AQP3* gene identified in eight SCZ patients were shown as blue bars. (b, c) *AQP3* expression levels in the cerebral cortex of *Plp-NF155*$^{Flox/Flox}$ (b, n = 4–5 mice each) and *CST-KO* mice (c, n = 4–5 mice each) were examined by qRT-PCR (*$p < 0.05$ compared to *Plp-NF155*$^{+/Flox}$ mice; Student's t-test). (d) Expression of *AQP3* mRNA (blue) was examined by *in situ* hybridization in the cerebral cortex of *Plp-NF155*$^{+/Flox}$ and *Plp-NF155*$^{Flox/Flox}$ mice 60 days after tamoxifen administration. Scale bar: 100 μm. (e) Cerebral cortices of *Plp-NF155*$^{+/Flox}$ and *Plp-NF155*$^{Flox/Flox}$ mice 60 days after tamoxifen administration were immunostained with anti-AQP3 (green) and anti-NeuN (red) antibodies. Higher-magnification view of the boxed area in the upper panel is shown in the lower panel. Arrows indicate AQP3-positive cells. Arrowheads indicate reduced AQP3 expression. Scale bar: 200 μm. (f) The percentages of AQP3$^+$/NeuN$^+$ double-positive cells were quantified in the upper and deeper layers of cerebral cortex of *Plp-NF155*$^{+/Flox}$ and *Plp-NF155*$^{Flox/Flox}$ mice (***$p < 0.001$ compared to AQP3$^+$/NeuN$^+$ double-positive group in *Plp-NF155*$^{+/Flox}$ mice; Student's t-test; n = 3 each). Abbreviations: SZ, schizophrenia; CONT, control. *NFX1, Nuclear transcription factor X-*

Box binding 1; AQP7, *Aquaporin 7; AQP3, Aquaporin 3; NOL6*, *Nucleolar protein 6; SUGT1P1, SGT1 homolog MIS12 kinetochore complex assembly cochaperone pseudogene 1; ANKRD18B, Ankyrin repeat domain 18B*. A one-sided Fisher's exact test was performed; $p = 0.042$.

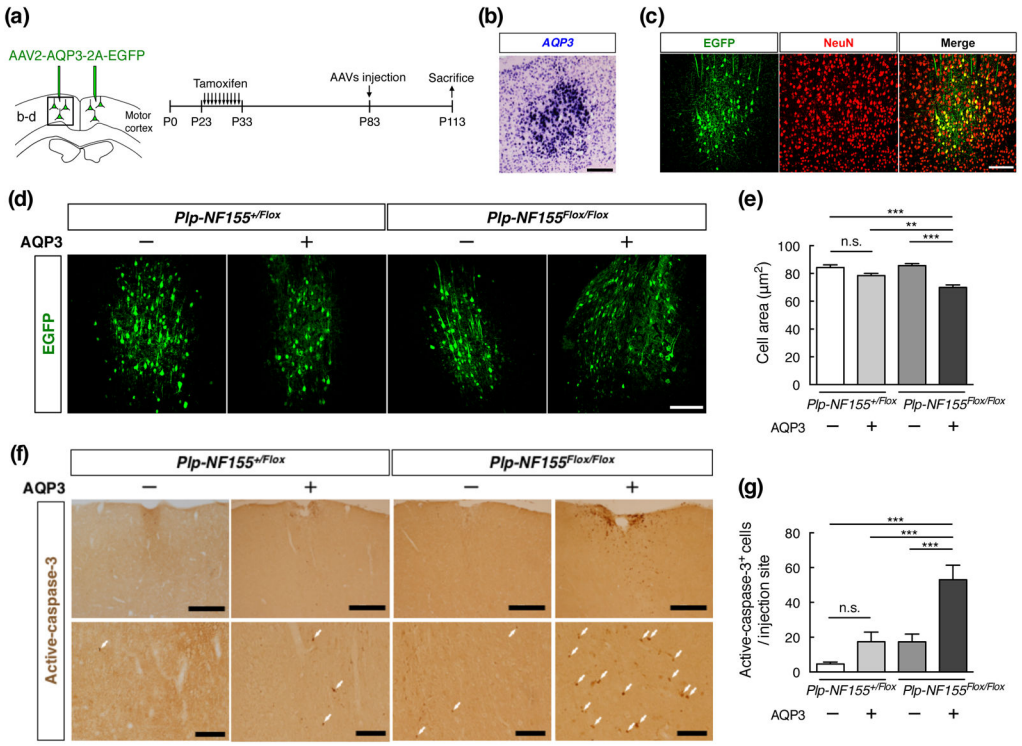

Fig. 4.

AAV-mediated overexpression of AQP3 induced caspase-3 activation in the motor cortex of *Plp-NF155*$^{Flox/Flox}$ mice. (a) Schematic drawing of the viral injections into the motor cortex and experimental time course. AAVs were injected into the motor cortex at P83 (50 days after tamoxifen treatment), and the tissues were collected at P113. (b) *In situ* hybridization for *AQP3* mRNA (blue) in the motor cortex of *Plp-NF155*$^{+/Flox}$ mice injected with AAV2-AQP3-2A-EGFP. Sections were counterstained with Nuclear Fast Red. Scale bar: 200 μm. (c) Representative images of immunostaining for EGFP (green) and NeuN (red) in the motor cortex of *Plp-NF155*$^{+/Flox}$ mice injected with AAV2- AQP3-2A-EGFP. Scale bar: 200 μm. (d) GFP^{+} neurons transduced with AAV2-EGFP- or AAV2-AQP3-2A-EGFP in the motor cortex of *Plp-NF155*$^{+/Flox}$ and *Plp-NF155*$^{Flox/Flox}$ mice. Scale bar: 200 μm. (e) Cell area was measured by EGFP fluorescence and ImageJ software for each genotype (**$p < 0.01$, ***$p < 0.001$ compared to *Plp-NF155*$^{Flox/Flox}$ + AAV2-AQP3-2A-EGFP group, one-way ANOVA followed by Tukey's post hoc tests; n.s., no significant difference compared to *Plp-NF155*$^{+/Flox}$ + AAV2-AQP3-2A-EGFP group, one-way ANOVA followed by Tukey's post hoc tests; n = 210–262 cells each). (f) The cerebral cortices of *Plp-NF155*$^{+/Flox}$ and *Plp-NF155*$^{Flox/Flox}$ mice injected with AAV2-EGFP or AAV2-AQP3-2A-EGFP were immunostained with anti-cleaved caspase-3 antibody (brown dots). Higher-magnification view of the boxed area in the upper panel is shown in the lower panel. Arrows indicate cleaved caspase-3^{+} signals. Scale bars: 200 μm (upper panel), 50 μm (lower panel). (g) The number of cleaved caspase-3^{+} cells at the injection site was counted in three sections per animal for each genotype (***$p < 0.001$ compared to *Plp-NF155*$^{Flox/Flox}$ + AAV2-AQP3-2A-EGFP group, one-way ANOVA followed by Tukey's post hoc tests; n.s., no

significant difference compared to *Plp-NF155*$^{+/Flox}$ + AAV2-AQP3-2A-EGFP group, one-way ANOVA followed by Tukey's post hoc tests; n = 6 mice each).

Table 1

Primer sequences used for RT-PCR and qRT-PCR.

Gene symbol	primer	sequences (5′to 3′)
DCN	Forward	GATTTTCCACCCGACACAAC
	Reverse	ATGAGGAACATTGGCCAGAC
MYH11	Forward	GTGACCTGCTTTTGGAGAGC
	Reverse	GCCTGTTCTTTGGTCTGAGC
PTTG1	Forward	TGGCTTCTAAGGATGGGTTG
	Reverse	GTGGCAATTCAACATCCAGA
DCT	Forward	TGTGCAAGATTGCCTGTCTC
	Reverse	GTTGCTCTGCGGTTAGGAAG
TTI2	Forward	TCACCTGTACATGCCTGAGC
	Reverse	CAGGGTTTCCAGGATCTTCA
AQP3	Forward	ATTCTGGCTATGCCGTCAAC
	Reverse	AAACTTGGTCCCTTGCCTTT
β-actin	Forward	TGACAGGATGCAGAAGGAGA
	Reverse	GCTGGAAGGTGGACAGTGAG
GAPDH	Forward	AACTTTGGCATTGTGGAAGG
	Reverse	ACACATTGGGGGTAGGAACA